High Temperature Corrosion of Materials (2023) 100:451–473
https://doi.org/10.1007/s11085-023-10197-9

REVIEW

Review on Strategies for Inhibiting Interdiffusion Between Protective Coatings and Superalloys Under High Temperature Oxidation

Bo Meng[1] · Jinlong Wang[1] · Zebin Bao[2] · Minghui Chen[1] · Shenglong Zhu[2] · Fuihui Wang[1,2]

Received: 29 July 2023 / Revised: 15 September 2023 / Accepted: 16 September 2023 /
Published online: 17 October 2023

Abstract

The service of protective coatings at high temperature will lead to interdiffusion between the coating and superalloy. The occurrence of interdiffusion not only reduces the oxidation resistance of the coating but also reduces the mechanical properties of superalloys, especially single crystal superalloys. At present, the main methods of suppressing interdiffusion are: adding a diffusion barrier layer between the coating and superalloy, a so-called "equilibrium" (EQ) coating, and a nanocrystalline coating. In the current review, the advantages and disadvantages of these three methods for suppressing interdiffusion are discussed, and an attempt is made to determine the best method for suppressing interdiffusion to improve the service life of high-temperature components.

Keywords Oxidation · Interdiffusion · Diffusion barrier · Nanocrystalline coating

✉ Jinlong Wang
wangjinlong@mail.neu.edu.cn

Bo Meng
1910132@stu.neu.edu.cn

Zebin Bao
zbbao@imr.ac.cn

Minghui Chen
mhchen@mail.neu.edu.cn

Shenglong Zhu
slzhu@imr.ac.cn

Fuihui Wang
fhwang@mail.neu.edu.cn

[1] Shenyang National Laboratory for Material Science, Northeastern University, Shenyang 110819, China

[2] Institute of Metal Research, Chinese Academy of Sciences, Shenyang 110016, China

Introduction

Nickel-based single crystal superalloys have been specifically developed for high-temperature applications in industrial gas turbines, aircraft, and jet engines [1–3]. The operating efficiency of the engine is closely related to the working stability. In other words, the higher the operating temperature of the engine, the higher the working efficiency. In order to improve the service life of superalloys, high-temperature protective coating technology must be applied, which can prevent the fast oxidation of superalloys.

Traditional aluminide coatings prepared by chemical vapor deposition (CVD) and MCrAlY (M = Ni and/or Co) overlay coatings prepared by physical vapor deposition (PVD) have been shown to enhance the oxidation resistance of superalloys at high temperatures [4–6]. Wang et al. [7] reported significant improvement in the oxidation resistance of cast Ni-based superalloy IN100 at 900 °C and 1000 °C using a NiCrAlY coating prepared by arc ion plating (AIP). The weight gain rate of IN100 is an order of magnitude higher than the one of NiCrAlY coating at 900 and 1000 °C. In another study, Xu et al. [8] investigated the high-temperature oxidation behavior of aluminide coating on Inconel 783 at 650, 750 and 850 °C for ultra-supercritical steam turbine application. The aluminide coating provided effective protection, significantly reducing the oxidation rate of the alloy. These high-temperature protective coatings are characterized by a high aluminum content, which acts as a source of aluminum for the formation of a protective α-Al_2O_3 scale on the component's surface.

Although aluminide coatings and MCrAlY coatings demonstrate excellent high-temperature oxidation resistance, they face significant challenges due to interdiffusion caused by the composition gradient with superalloys [9–13]. This interdiffusion primarily involves the diffusion of Al and Cr from the coating into the superalloy and the diffusion of the alloy elements (Ni, Co and refractory elements) from the superalloy into the coating. The affected regions in superalloy substrates due to interdiffusion are categorized into two zones [14, 15]: The interdiffusion zone (IDZ) and the secondary reaction zone (SRZ). The IDZ is located near the interface between the coating and the superalloy, while the SRZ forms beneath the IDZ and encompasses a recrystallized substrate with a high density of needle-like topologically closed-packed (TCP) phases. The formation of the TCP phases is caused by the precipitation of refractory elements (Mo, W, and Re) in the γ matrix phases [14, 16]. Both the diffusion of Ni to the coating and diffusion of Al to the substrate will transform γ-Ni phases into γ'-Ni_3Al phases, resulting in the precipitation of refractory elements. Hence, the formation of TCP phases can adversely impact the mechanical properties of nickel-based single crystal superalloys [17–21]. Simonetti et al. [22] observed that the precipitation of TCP phases can affect the creep strength by disturbing the regularity of the γ/γ' rafted microstructure. Research by Sugui et al. [23] demonstrated that an increase in the content of W and Re in single crystal superalloys leads to an increase in TCP phase formation, resulting in reduced creep strength and service life.

In general, interdiffusion resulting from differences in the chemical compositions of coatings and superalloys can significantly impact the service life of components. Therefore, finding solutions to suppress interdiffusion have become an urgent need. The current review paper provides a concise overview of approaches to mitigate interdiffusion arising from the distinct chemical compositions of high-temperature protective coatings and superalloys. Among them, the development of a diffusion barrier is considered to be one of the most direct and effective methods.

The Hazards of Interdiffusion

The hazards caused by the interdiffusion mainly include reducing the oxidation resistance of the coating and reducing the mechanical properties of the superalloy.

As interdiffusion occurs, the concentrations of Ni and Al in the coating increase and decrease, respectively. The increase in Ni concentration and the decrease in Al concentration will transform the β-NiAl into the γ-Ni and the oxidation resistance of γ-Ni is lower than that of β-NiAl [24].

More importantly, interdiffusion can degrade the mechanical properties of superalloys. This can be mainly explained from three aspects:

(1) Precipitation of refractory elements: Re, W, Mo, and other refractory elements exhibit the strongest solid solution strengthening effect in superalloys. This strengthening is mainly achieved through the lattice distortion caused by the size difference between these elements and Ni. Additionally, the addition of these elements reduces the stacking fault energy of the face-centered cubic matrix, making it easier for dislocations generated during deformation to decompose into extended dislocations. This restricts the movement of dislocations and thus, increases the strength of the matrix [25]. Therefore, the precipitation of refractory elements reduces the mechanical properties of superalloys;
(2) Destruction of the γ/γ': The cubic γ'-Ni_3Al phases in superalloys is arranged in an orderly array, and they are often coherent with the matrix γ-Ni phase to play a role in precipitation strengthening. Destruction of the γ/γ' structure reduces the mechanical properties of superalloys [26];
(3) The formation of TCP phases: The formation of the TCP phase not only increases the crack sensitivity but also accelerates crack propagation [22, 23].

Sato et al. [27] investigated the influence of interdiffusion on the high-temperature creep performance of superalloys, which were coated with aluminum diffusion coatings. Experimental results indicated that the creep-rupture lives of coated superalloys were shorter than those of the bare superalloys, as depicted in Fig. 1. In particular, the coated superalloy TMS-138 had an 86% reduction in creep-rupture life, which had the widest zone affected by interdiffusion.

In addition, Kirkendall voids are easily formed at the interface between the coating and the superalloy, which is caused by interdiffusion. During the interdiffusion process, the number of Ni atoms and other types of atoms that diffuse out is relatively large,

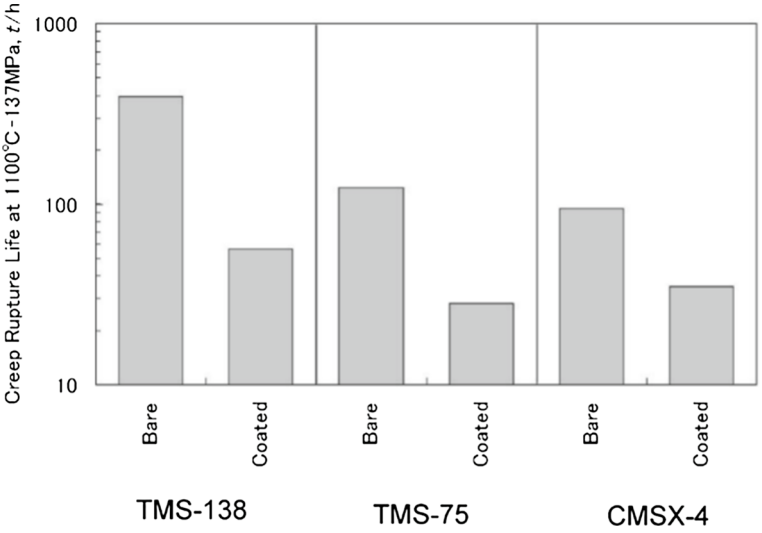

Fig. 1 Creep rupture life at 1100 °C–137 MPa of the bare and coated TMS-138, TMS-75 and CMSX-4 [27]. Reproduced from Refs. [27] with permission from the Japan Institute of Metals and Materials

and the number of Al atoms that diffuse into the matrix is not enough to supplement the number of Ni, Co, Cr, Mo and other elements that diffuse from the superalloys into the coating. Therefore, Kirkendall voids are formed near the interface between coatings and superalloys.

In general, interdiffusion poses significant challenges to coatings and superalloys. Finding methods to inhibit interdiffusion between elements are currently a top priority.

Diffusion Barrier System

Concept

In order to solve the issue of reduced coating life and alloy mechanical properties caused by interdiffusion, extensive research has been conducted in the field, with a strong emphasis on improving coating structure and activity, as well as enhancing interfacial diffusion resistance, etc. Among them, the development of diffusion barrier is considered to be one of the most direct and effective methods [28–30].

The diffusion barrier coating system comprises an alloy superalloy, a diffusion barrier layer, and a high-temperature protective coating, as illustrated in Fig. 2. According to Fick′s first law, the diffusion flux J_{Al} of Al through the barrier layer is given by the following Eq. (1) [31]:

$$J_{Al} = D_{Al}\delta C_{Al}/\delta_x \tag{1}$$

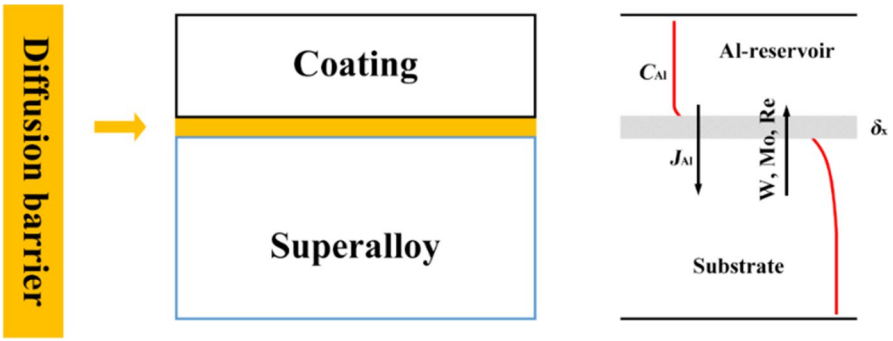

Fig. 2 Schematic diagram of the structure of the diffusion barrier system

where D_{Al} and S_{Al} are the diffusion coefficient and solubility limit of Al in the barrier layer, respectively. C_{Al} is the concentration of Al in the coating. The driving force $\delta C_{Al}/\delta_x$ will be given by the concentration difference across the barrier δC_{Al} divided by the thickness of the barrier layer δ_x. According to Eq. (1), a slow diffusion flux can be obtained by using low values of D_{Al} and S_{Al}. Therefore, it is crucial to select a barrier coating with low D_{Al} and S_{Al}.

An effective diffusion barrier should meet the following three conditions: (1) the diffusion rate of Al or matrix element in it is low; (2) good temperature stability; (3) excellent bonding force with the coating and the superalloy. Diffusion barriers are generally divided into two categories: ceramic diffusion barriers and metal diffusion barriers.

Ceramic Diffusion Barrier

Ceramic materials have great potential as diffusion barriers due to good high-temperature stability and reduced diffusion coefficients. The main reasons for the low diffusion coefficient of elements in ceramic materials are [32–34]:

(1) Crystal structure: Ceramics have a highly ordered and tightly packed crystal structure. The atoms or ions are arranged in a specific pattern, which limits the movement of atoms and slows down diffusion. The regular arrangement of atoms makes it difficult for them to move and find open spaces to diffuse;
(2) Strong atomic bonding: Ceramic materials have strong chemical bonds between atoms or ions, such as ionic or covalent bonds. These bonds require a significant amount of energy to break, hindering the movement of atoms and reducing the diffusion rate. The high bond strength results in higher activation energy required for atoms to migrate through the crystal lattice;
(3) Lack of free vacancies: Diffusion in ceramics relies on the availability of vacancies, which are empty spaces within the crystal lattice. However, ceramics tend to have a low number of vacancies compared to metals or polymers. This scarcity of vacancies restricts the movement of atoms, resulting in slower diffusion rates;

(4) Defects and impurities: Ceramic materials typically have fewer defects and impurities compared to other materials. Defects, such as dislocations, grain boundaries, or vacancies, can act as diffusion paths for atoms. The limited presence of such defects in ceramics restricts the pathways available for atom diffusion and slows down the diffusion process.

Nitride ceramics were among the earliest ceramic materials used as diffusion barriers. Zhu et al. [35] applied a 400 nm AlN diffusion barrier layer to the nickel-based superalloy K417/Ni + CrAlYSiN coating system. The AlN diffusion barrier layer prepared using AIP is formed by reacting a pure aluminum target with nitrogen gas. After exposure at 1000 °C for 100 h, the AlN diffusion barrier layer effectively hindered the diffusion, as depicted in Fig. 3. Moreover, the oxide scale formed on the coating surface consisted of pure α-Al_2O_3. In contrast, the coating without the AlN diffusion barrier exhibited a two-layered oxide scale: an inner layer of α-Al_2O_3 and an outer layer of $NiCr_2O_4$. The diffusion of Al into the substrate in the coating without AlN diffusion barrier layer leads to a decrease in the coating oxidation resistance. Zhu et al. [36] also introduced TiN as a diffusion barrier layer between the Ni + CrAlYSiN coating and the superalloy K417. The

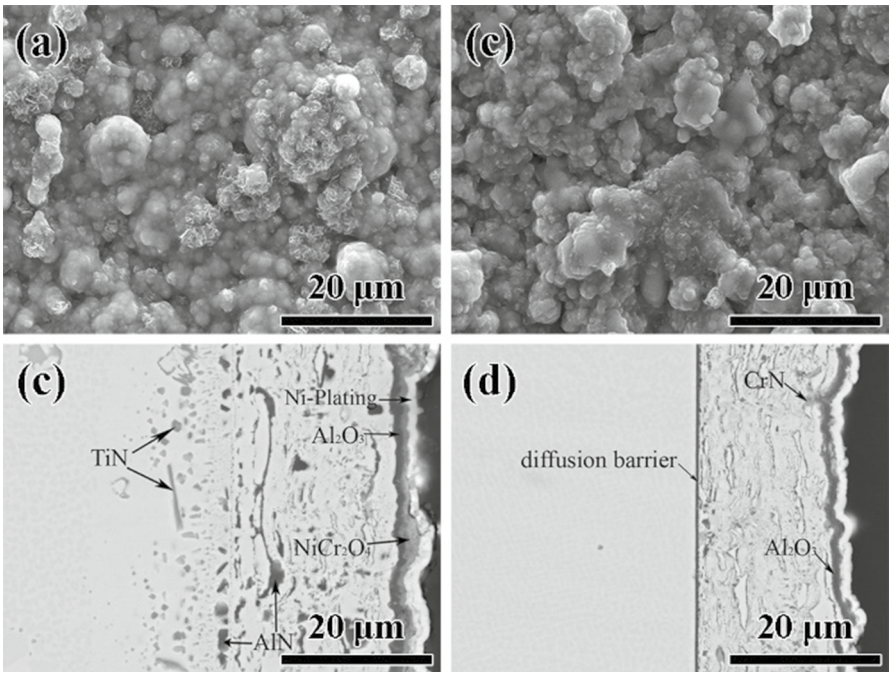

Fig. 3 Surface SEM image of **a** coating system without AlN diffusion barrier, **b** coating system with AlN diffusion barrier; and cross-sectional BSE images of **c** coating system without AlN diffusion barrier, **d** coating system with AlN diffusion barrier [35]. Reproduced from Refs. [35] with permission from the Corrosion Science©2012, Elsevier

results demonstrated that it did not improve the oxidation resistance of the coating, although the TiN diffusion barrier layer inhibits the interdiffusion.

Li et al. [37] applied a CrN diffusion barrier between the NiCrAlY coating and the superalloy DSM11, also by AIP. The inclusion of the CrN interlayer effectively restrained the interdiffusion between the NiCrAlY coating and the superalloy DSM11. This phenomenon can be attributed to the occurrence of interdiffusion reactions within the diffusion barrier during vacuum heat treatment and high-temperature exposure.

The ionic bonds between metal cations and oxyanions are typically stronger in oxide ceramics than in nitride ceramics, leading to higher energy barriers for atomic diffusion. Consequently, diffusion coefficients are generally smaller in oxide ceramics when compared to nitride ceramics. In other words, oxides diffusion barriers are more effective in inhibiting diffusion than nitrides diffusion barriers.

Li et al. [38] conducted a study in which they prepared CrO150N and CrO50N as diffusion barriers between the NiCrAlY coating and the superalloy DSM11 using AIP. The diffusion barriers were deposited from a pure Cr target in a reactive atmosphere ($N_2 + O_2$). Two different O_2 flow rates were used, 150 ml/min and 50 ml/min. The CrON diffusion barriers consisted of both Cr_2O_3 and CrN phases. The CrO150N diffusion barrier exhibited a columnar structure and had a higher Cr_2O_3/CrN ratio compared to the CrO50N diffusion barrier. Notably, the NiCrAlY coating with the CrO50N diffusion barrier displayed superior oxidation resistance when compared to the coating without the CrO150N diffusion barrier. This improved performance was attributed to the slower depletion of Al in the coating. The enhanced barrier ability of the CrO50N diffusion barrier can be attributed to its lower density of defects. Additionally, the CrO50N diffusion barrier effectively addressed the limitations of CrN in hindering the in-diffusion of Al.

Peng et al. [39] conducted a study where they prepared an α-Al_2O_3 diffusion barrier layer by controlling the oxygen influx rate during the deposition of NiCoCrAlY coating on the nickel-based superalloy DZ125 using electron beam physical vapor deposition (EB-PVD). The findings demonstrated that α-Al_2O_3 effectively hindered the diffusion of elements, as depicted in Fig. 4.

Cremer et al. [40] prepared an Al-O-N diffusion barrier layer between the nickel-based superalloy CMSX-4 and MCrAlY coatings using magnetron sputtering. Following annealing at 1100 °C for 4 h, the Al-O-N diffusion barrier remained in an amorphous state, while the nanocrystalline γ-Al_2O_3 transformed into crystalline α-Al_2O_3. Notably, there was no observed diffusion of Ti, Ta and W from superalloy CMSX-4 into the Al-O-N or MCrAlY coating. These results indicate that Al-O-N is highly effective as a diffusion barrier at 1373 K.

Knotek et al. [41] prepared a Ti–Al-O diffusion barrier layer using magnetron sputtering in a nickel-based superalloy (CMSX-6, IN100)/MCrAlY coating system. Their findings revealed that the stable amorphous structure of the Al-O-N layer, with a thickness of 1–1.5 µm, effectively prevented interdiffusion between the coating and the base alloy even after annealing at 1100 °C for over 400 h. However, the bonding strength of the Al-O-N layer within the system still requires further enhancement.

Although oxide diffusion barriers are effective in inhibiting interdiffusion, they have poor adhesion to coatings and superalloys. In addition, their coefficient of

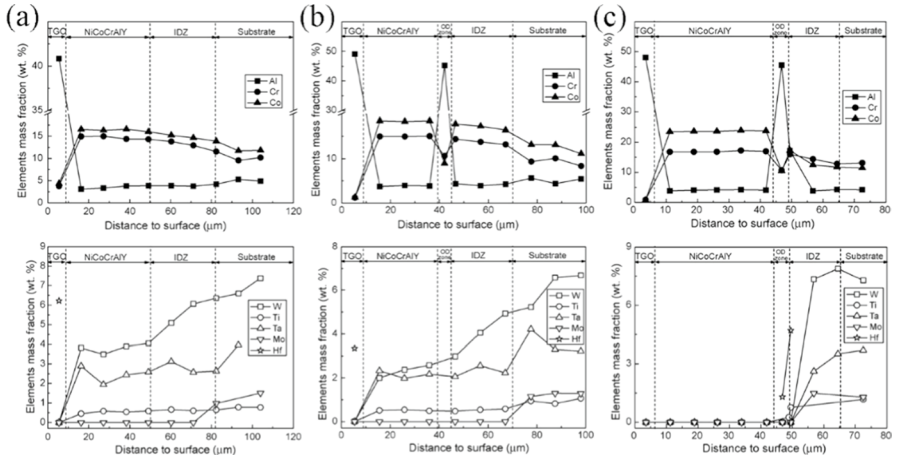

Fig. 4 Element distribution across the thickness of the coated specimens after oxidation at 1323 K for 160 h: **a** NiCoCrAlY; **b** OD NiCoCrAlY (100 sccm); **c** OD NiCoCrAlY (300 sccm) [39]. Reproduced from Refs. [39] with permission from the Journal of Alloys and Compounds©2010, Elsevier

thermal expansion (CTE) is much lower than that of metallic coatings and superalloys, which would easily result in the delamination of the protective coating during the high-temperature service. Müller et al. [42] reported that the α-Al_2O_3 diffusion barrier successfully prevented noticeable interdiffusion between superalloy CMSX-4 and NiCoCrAlY coating, but the adhesion still requires improvement. Similarly, Knotek et al. [43] highlighted the need to strengthen the bonding force of the Al-O-N diffusion barrier in the CMSX-6/NiCrAlY system. To address the bonding force issue between superalloys and coatings, gradient diffusion barriers and self-formed diffusion barriers have been developed.

Ren et al. [44] developed a NiCrAlYSiHf coating on K417G using magnetron sputtering. After post-annealing, the coating consisted of γ'-Ni_3Al matrix and α-Cr precipitates. Notably, no coating spallation was observed even after subjecting the coating to 100 cycles of a water-quenching test ranging from 1000 to 25 °C. During high-temperature exposure, a continuous $Cr_{23}C_6$ interlayer spontaneously formed between the coating and the superalloy. This interlayer effectively suppressed interdiffusion between the coating and the superalloy, as demonstrated in Fig. 5.

In order to enhance the bonding force of the Al–O–N diffusion barrier in the CMSX-6/NiCrAlY system, Knotek et al. [43] incorporated Cr to create a Cr-Al-O-N diffusion barrier by magnetron sputtering. The introduction of Cr leads to the formation of tooth-like oxide precipitations through a reaction with Al present in the coating/substrate interface. Tooth-like oxide precipitation is similar to oxide pegging. This reaction significantly enhanced the bonding force of the diffusion barrier within the CMSX-6/NiCrAlY system.

Cai et al. [45] deposited a gradient Zr/ZrN/Zr layer as a diffusion barrier between the NiCrAlYSi coating and the nickel-based superalloy DZ125. The gradient Zr/ZrN/Zr diffusion barrier layers were prepared by AIP. The results demonstrated that this diffusion barrier exhibited excellent oxidation resistance when oxidized at

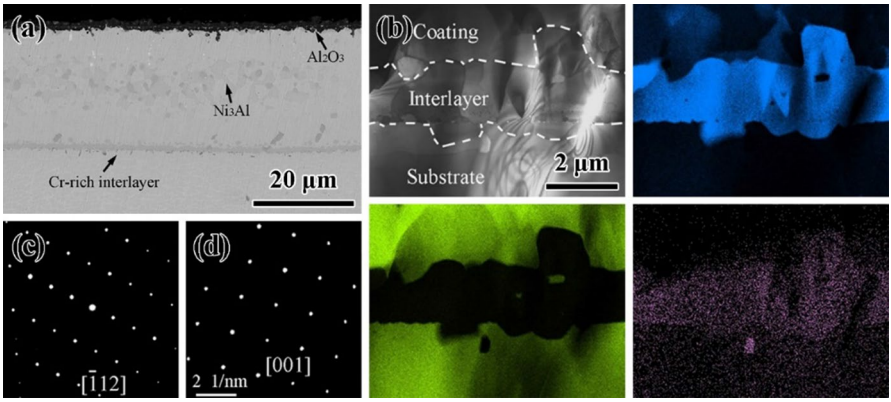

Fig. 5 **a** Cross-sectional BSE image of the coating after 100 cyclic thermal shock at 1000 °C; **b** element mapping of Cr, Ni and Cr-rich interlayer; **c** and **d** SAD patterns of Cr-rich interlayer [44]. Reproduced from Refs. [44] with permission from the Corrosion Science©2015, Elsevier

1100 °C. However, it is important to note that nickel-based superalloys do not typically contain Zr. Consequently, over prolonged exposure to high temperatures, Zr from the diffusion barrier may diffuse into the nickel-based superalloys, leading to a decline in their mechanical properties.

In summary, ceramic diffusion barriers typically exhibit effective performance in hindering the diffusion of elements between coatings and superalloys. However, the application of ceramic diffusion barriers is somewhat restricted, particularly in cases involving long-term thermal shocks at high temperatures, which can result in coating cracking or decomposition failure.

Metal Diffusion Barrier

Compared with ceramic diffusion barriers, metal diffusion barriers have better adhesion to coatings and superalloys. The main reasons are:

(1) Coherence type: The combination of the metal diffusion barrier with the coating and superalloy belongs to the metallic coherence, after exposure at high temperatures;
(2) Coefficient of thermal expansion: Compared with ceramic, metallic diffusion barriers have less thermal expansion coefficient mismatch with coatings and superalloys. Coefficient of thermal expansion mismatch leads to the formation of thermal stress in the diffusion barrier, according to Eq. (2) [46–48]:

$$\sigma_{\mathrm{th}} = \frac{E_{\mathrm{DB}}(\alpha_{\mathrm{DB}} - \alpha_{\mathrm{metal}})}{1 - \nu_{\mathrm{DB}}} \tag{2}$$

where E_{DB} is Young's modulus of diffusion barrier; ν_{DB} is the Poisson's ratio of diffusion; α_{DB} and α_{metal} are the CTEs of the diffusion barrier and coating or

superalloy, respectively; and ΔT is the temperature difference between the oxidation temperature and the room temperature. Hence, Therefore, the thermal stress caused by the mismatch of CTE in the metal diffusion barrier is smaller.

Metal diffusion barriers primarily consist of refractory metals, such as Ta, Re, Ru. This choice is mainly due to the small diffusion coefficient of elements in refractory metals. Currently, Ru is the most commonly used metal diffusion barrier material. In a study reported by Bai et al. [49], a layer of Ru was electroplated as a diffusion barrier between the first-generation single crystal superalloy DD3 and NiAlDy coatings. High temperature oxidation behavior of this system was investigated at 1100 °C. The results demonstrated that the utilization of a Ru diffusion barrier effectively hindered the interdiffusion between the coating and the substrate. Notably, no SRZ formed in the DD3 single crystal substrate, and the high-temperature oxidation resistance of the coating was improved. Because the formation of SRZ is caused by interdiffusion, where Al in the coating diffuses into the superalloy. This reduces the oxidation resistance of the coating. Thus, inhibiting the formation of SRZ will improve the oxidation resistance. We have added it in the manuscript.

Katsumata et al. [50] electroplated a Re diffusion barrier in the Hastelloy-X/NiAl system. After 100 h of oxidation, the diffusion barrier coating system exhibited a duplex structure comprising an inner σ-(Re, Mo, Cr, Ni) layer and an outer β-NiAl layer, covered by a protective Al_2O_3 scale. In contrast, the NiAl coating degraded, forming a reaction diffusion zone of γ-Ni(Cr, Mo, Fe, Al) with voids, while the external scale extensively spalled. After 400 h of oxidation, an intermediate reaction–diffusion zone was observed in the diffusion barrier coating system. The Mo present in the alloy substrate enriched the inner σ-layer, transforming it from a Re-based alloy to a Mo-based alloy. The Mo-based alloy appeared to facilitate both inward diffusion of Al and outward diffusion of alloying elements such as Mo, Fe and Cr, resulting in the formation of the intermediate reaction–diffusion zone.

Considering the susceptibility of sing-component metal diffusion barriers to decomposition at high temperatures, researchers have turned to the development of two-component and multi-component diffusion barrier systems. These systems often incorporate refractory elements, such as Ta–Nb, Ta–Ir and W–Ni. Burman et al. [51, 52] prepared metal Ta and Nb diffusion barriers by vacuum plasma spraying and sputtering techniques. It was observed that a single Ta or Nb diffusion barrier alone could not effectively hinder the diffusion of elements such as Ni and Fe. Moreover, the presence of Ta or Nb diffusion barriers had an impact on the bond strength of coatings during thermal shock tests, resulting in cracking after a few cycles, specifically between the diffusion barrier and the substrate. However, the introduction of a Nb–Ta diffusion barrier led to the formation of intermediate compounds, such as Fe_3Ta_7 and Ni_3Ta, which exhibited an improved diffusion barrier effect.

Wu et al. [53] prepared a diffusion barrier layer of Ta-Ir in the nickel-based superalloy TMS-75/aluminide coating system. The incorporation of the Ta-Ir diffusion barrier resulted in enhanced cyclic oxidation resistance of the aluminized coating at 1100 °C. Notably, the depth of distribution of TCP phases was reduced from 300 to 180 μm, as illustrated in Fig. 6.

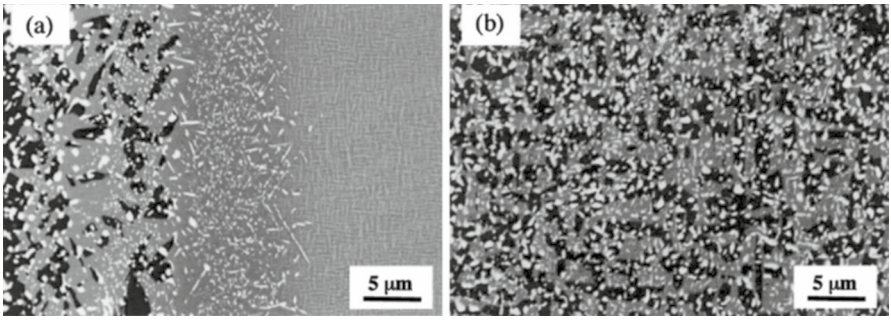

Fig. 6 SEM images of the cross-sectional microstructure. **a** Ir-Ta-Al coated TMS-75, and the observed area is approximately 180 μm in depth from the surface; **b** simply aluminized TMS-75, and the observed area is approximately 300 μm in depth from the surface [53]. Reproduced from Refs. [53] with permission from the Surface and Coatings Technology ©2003, Elsevier

Cavaletti et al. [54] investigated the impact of a Ni–W electrolytic diffusion barrier layer on the oxidation behavior of the MCNG/Pt-modified aluminide coating system at 1100 °C. While the Ni–W diffusion barrier effectively suppressed interdiffusion, the inclusion of W resulted in a reduction in oxidation resistance, as depicted in Fig. 7. The main reason for the decrease in oxidation resistance is that the solubility of W in the bonding coating is quite high, resulting in low purity of the oxide scale formed on bonding coating. In addition, the volatility of W oxide leads to reduced adhesion of the oxide scale.

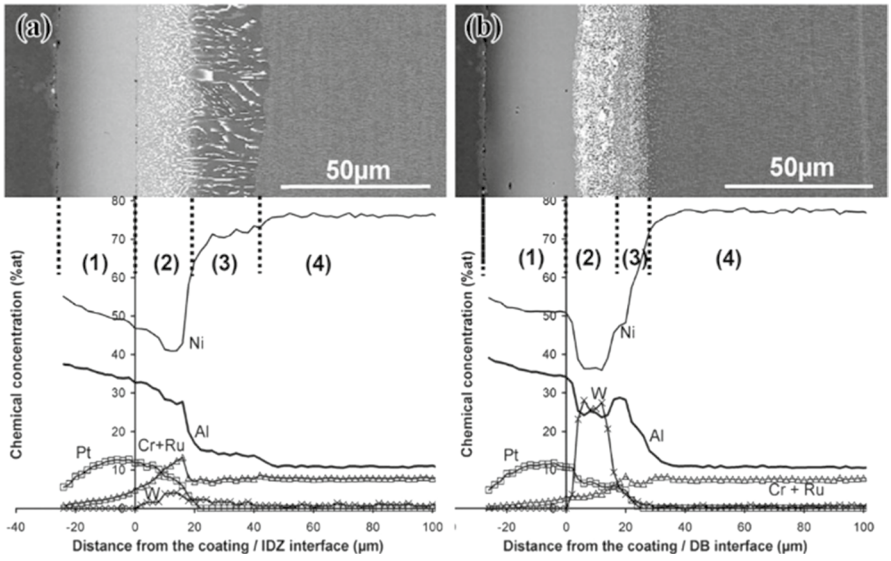

Fig. 7 Microstructure and chemical composition of the systems without (**a**) and with a DB (**b**) [54]. Reproduced from Refs. [54] with permission from the Surface and Coatings Technology ©2009, Elsevier

The multi-component diffusion barrier is mainly Re–Cr–Ni–Ta/Mo/W system. Lang et al. [55] electroplated a Re–Cr–Ni–Mo diffusion barrier in the nickel-based superalloy IC6/aluminide coating system. The presence of this diffusion barrier significantly reduced the depth of the IDZ from 200 to 15 μm in the superalloy IC6. Moreover, it led to improved oxidation resistance of the coating. Similarly, Narita et al. [56] examined the impact of a Re(W)–Cr–Ni diffusion barrier on the oxidation behavior of the TMS-82/aluminide coating system at 1150 °C. The incorporation of W in the diffusion barrier resulted in a reduction in the Cr content, thereby enhancing the ability of diffusion barrier to prevent diffusion.

In addition to refractory metal, high-entropy alloys also show promising potential as thermal barrier layers. High-entropy alloys are composed of five or more metal elements, with approximately equal mole fractions of each element. One key advantage of high-entropy alloy is their slow diffusion rate, which is a critical characteristic for an effective diffusion barrier. Xu et al. [57] deposited an AlCrCoNiMo high-entropy alloy diffusion barrier between a NiAlHf coating and the N5 superalloy. The AlCrCoNiMo high-entropy alloy diffusion barrier effectively prevented the formation of IDZ, SRZ, and TCP phases in the superalloy N5, as demonstrated in Fig. 8. This can be attributed to the significantly reduced diffusion coefficients of alloying elements (such as Re) and Al in the AlCrCoNiMo high-entropy alloy diffusion barrier, as shown in Table 1. Furthermore, Xu et al. [57] also investigated

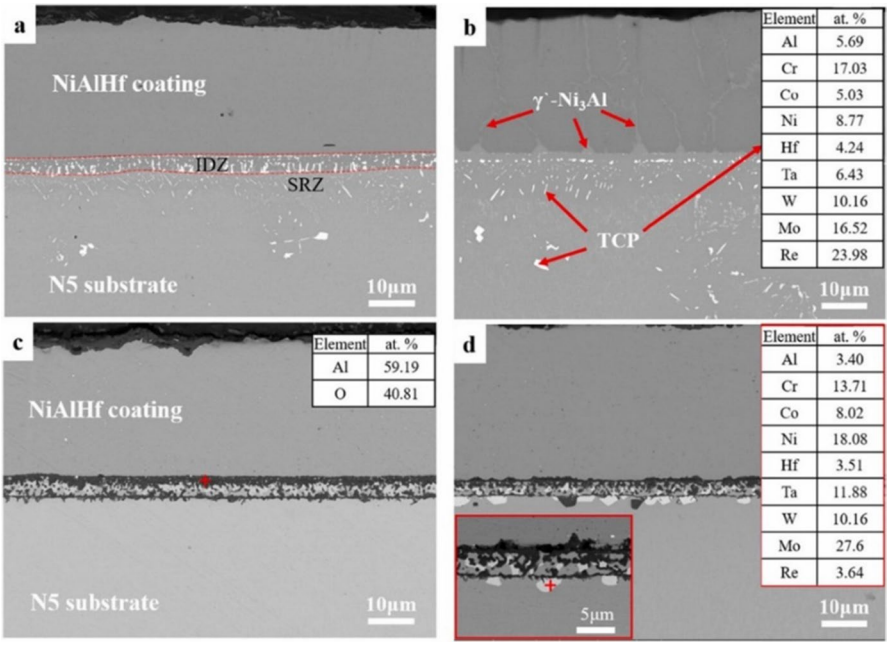

Fig. 8 Cross-sectional morphologies of the specimens after static isothermal oxidation 1373 K: NiAlHf/N5 specimen after **a** 50 h and **b** 100 h oxidation; NiAlHf/AlCrCoNiMo/N5 specimen **c** 50 h and **d** 100 h oxidation [57]. Reproduced from Refs. [57] with permission from the Surface and Coatings Technology ©2021, Elsevier

Table 1 Diffusion coefficients of Al and alloying elements (Re) in the NiAlHf coating and NiAlHf/AlCrCoNiMo coating at 1373 K [57]

Diffusion coefficient	NiAlHf	NiAlHf/AlCrCoNiMo
Al	10^{-14} m^2/s	10^{-17} m^2/s
Re	10^{-14} m^2/s	10^{-20} m^2/s

the use of an AlTiCrNiMo high-entropy alloy diffusion barrier. Although it did not entirely inhibit the formation of IDZ, it successfully limited the width of the interdiffusion zone to approximately 10 μm.

In summary, metal diffusion barriers have advantages in terms of adhesion to alloys or coatings. However, their performance in hindering diffusion is generally less effective compared to ceramic diffusion barriers. Metal diffusion barriers may be difficult to completely suppress the interdiffusion of elements. Additionally, metallic diffusion barriers are more susceptible to decomposition failure compared to ceramic diffusion barriers.

Equilibrium Coating

In order to solve the issue of interdiffusion caused by the chemical potential difference between coatings and single crystal superalloys, Japanese researchers have proposed and developed a phase equilibrium (EQ) coating. The concept behind EQ coatings is based on achieving a γ and γ' phase equilibrium state in nickel-based single crystal superalloys. The coating is designed to predominantly consist of the γ' phase, aligning the chemical potential of the elements in the coating with that of the superalloy. This approach effectively inhibits interdiffusion between the superalloy and the coating.

Different coatings including NiCrAlY, γ phase and γ' phase were applied to the superalloy TMS-82+ by Sato et al. [58]. Experimental testing was conducted at 1100 °C, and the results revealed the formation of an IDZ with a width of approximately 150 μm and an SRZ with a width of 85 μm in the superalloy with NiCrAlY coating. However, in the case of the superalloy with the γ phase coating, the IDZ width was reduced to 5 μm, and for the superalloy with the γ' phase coating, the IDZ width was further reduced to 20 μm. These findings indicate that the γ and γ' phase coatings effectively inhibit the diffusion of elements and minimize the extent of interdiffusion between the superalloy and the coating.

In another study, EQ coating and NiCrAlY coating were applied on TMS-138 single crystal superalloy for comparative experiments by Kawagishi et al. [59]. The coatings were prepared by HVOF technology and the nominal compositions of substrates and coatings are shown in Table 2. The results showed that the EQ coating not only effectively inhibited the formation of the SRZ, but also ensured that the creep strengthening the performance of the superalloy TMS-138 remained unaffected. This is illustrated in Fig. 9, where the EQ coating demonstrated superior performance in terms of

Table 2 Nominal compositions of substrates and coatings [59]

	Co	Cr	Mo	W	Al	Ta	Hf	Re	Ru	Y
TMS-138	5.9	2.9	2.9	5.9	5.9	5.9	0.1	4.9	2.0	
TMS-138A	5.8	3.2	2.8	5.6	5.7	5.6	0.1	5.8	3.6	
TMS-196	5.6	4.6	2.4	5.0	5.6	5.6	0.1	6.4	5.0	
TMS-138γ′	4.3	1.5	1.6	5.5	8.3	8.5	0.1	1.8	1.5	
TMS-138A γ′	4.3	1.6	1.5	5.3	8.1	8.2	0.2	2.1	2.8	
TMS-196 γ′	4.2	2.4	1.3	4.8	7.7	8.1	0.1	2.3	3.9	
TMBC-1	6.2	4.0	1.0	4.5	8.1	9.9	0.4			0.1
Amdry9954	38.5	21.0			8.0					0.5

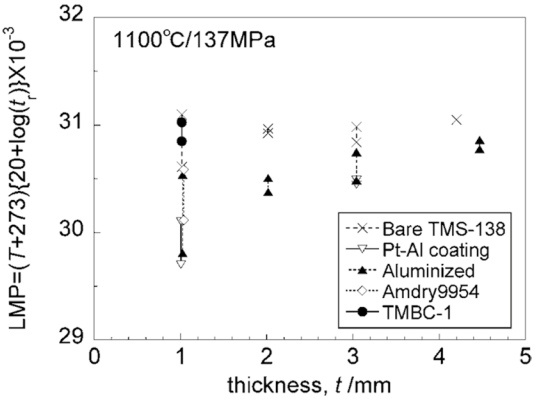

Fig. 9 Larson-Miller parameter distribution with various thicknesses of creep specimens for bare and coated TMS-138 [59]. Reproduced from Refs. [59] with permission from the Japan Institute of Metals and Materials

both interdiffusion suppression and maintaining the creep strength of the single crystal superalloy TMS-138.

While the preparation process of γ phase and/or γ' phase EQ coatings has become relatively mature and can effectively inhibit interdiffusion between the coating matrix and the substrate, there are still some limitations compared to traditional MCrAlY coatings and aluminide coatings. One major drawback of EQ coatings is their insufficient high-temperature oxidation resistance. During prolonged high-temperature service, EQ coatings tend to degrade. This is primarily due to the low Al content in the EQ coating, which cannot provide a sustained source of Al for the formation of a protective α-Al_2O_3 scale over an extended period. As a result, the protective oxide scale may not adequately form or may not be able to maintain its integrity, leading to decreased oxidation resistance of the EQ coating.

Nanocrystalline Coating

Concept

The development of diffusion barriers and EQ coatings has indeed been effective in inhibiting the formation of SRZ and TCP phases resulting from interdiffusion between high-temperature protective coatings and superalloys. However, interdiffusion between coatings and superalloys still cannot be completely suppressed.

To solve this issue, Wang et al. [60] introduced the concept of nanocrystalline coatings. These coatings consist of a columnar structure with the same chemical composition as the superalloy and are prepared through magnetron sputtering. The nanocrystalline coating exhibits several advantages over traditional metal coatings, including the presence of numerous straight grain boundaries. These grain boundaries provide rapid diffusion paths for Al and promote the formation of protective alumina scales at the surface. Consequently, the nanocrystalline coating shows promise in mitigating interdiffusion-related issues between the coating and the superalloy.

According to Wagner's theory, the critical concentration of Al for the formation of an external α-Al_2O_3 scale is expressed as [61]:

$$N_{Al}^{*} = \left(\frac{3\pi g^{*} N_O D_O V_M}{4 D_{Al} V_{OX}} \right)^{1/2} \tag{3}$$

where N_{Al}^{*} is the critical concentration of Al, $N_O D_O$ is the oxygen permeability, D_{Al} is the diffusivity of Al, g^{*} is a factor determined by the volume fraction of α-Al_2O_3 required for the formation of an external scale, and V_M and V_{OX} are mole volumes of the coating and oxide α-Al_2O_3, respectively. Equation (3) can be simplified as follows:

$$N_{Al}^{*} \propto D_{Al}^{-1/2} \tag{4}$$

The diffusivity of Al in metal is the sum of grain boundary diffusivity (D_L) and lattice diffusivity (D_{GB}). The grain size has a decisive influence on the diffusion coefficient of the Al in the coating, according to Eq. (5) [62]:

$$D_{Al} = (1 - f) D_L + f D_{GB} \tag{5}$$

where f is the area proportion of the grain boundary. Assuming the grains in coatings are cubic, $f = 2\delta/d$ (δ is the GB width and d is the grain size). Also, considering $D_{GB} \gg D_L$, Eq. (6) can be simplified as follows:

$$D_{Al} = D_L + \frac{2\delta}{d} D_{GB} \tag{6}$$

Considering that Al diffuses mainly through grain boundaries ($(2\delta/d) \cdot D_{GB}$) at high temperatures, the relationship between the critical Al content and the grain size is expressed by Eq. (7):

$$N_{Al}^{*} \propto d^{-1/2} \tag{7}$$

Therefore, grain refinement can reduce the critical Al concentration for the formation of the α-Al_2O_3 scale. Figure 10 depicts the microstructure of the nanocrystalline coating, showcasing the columnar grain structure. The width of the columnar grains in the coating is approximately 50 µm.

Inhibition of Interdiffusion

The nanocrystalline coating, with its chemical composition matching that of the superalloy, offers a comprehensive solution to the problem of interdiffusion between the coating and the superalloy.

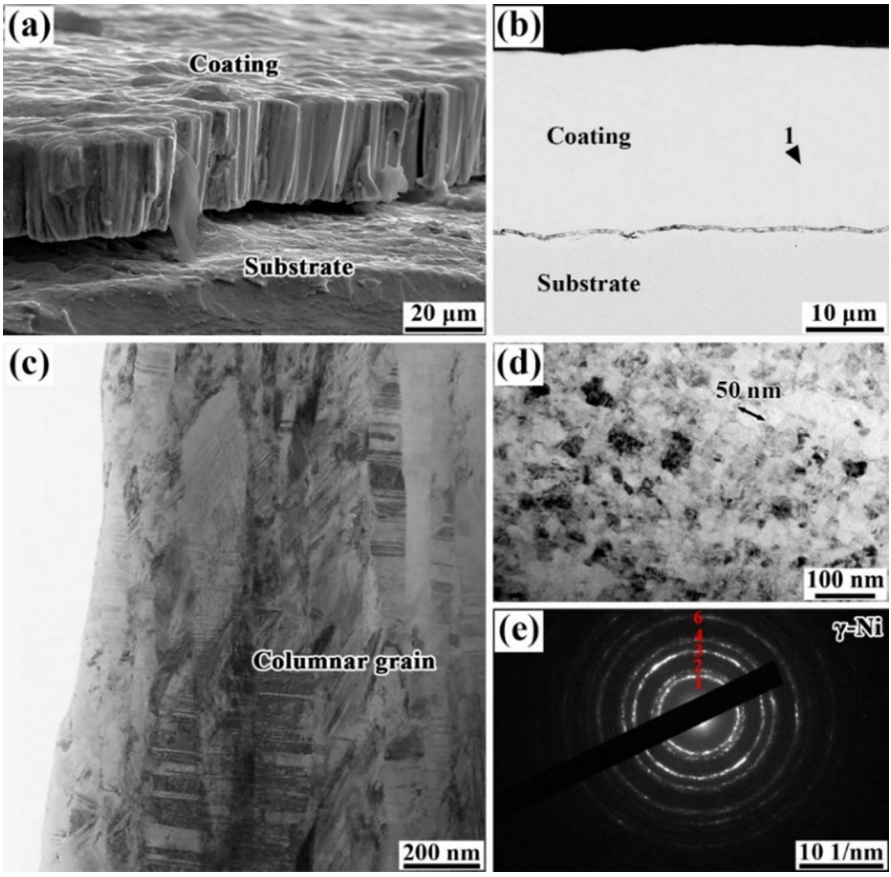

Fig.10 Typical microstructures of the as-deposited nanocrystalline coating: **a** fractured morphology; **b** cross-sectional morphology by SEM; **c** the cross-sectional and **d** plan-view morphologies by TEM bright field and **e** the corresponding SAED patterns [63]. Reproduced from Refs. [63] with permission from the Journal of Materials Science & Technology ©2023, Elsevier

Wang et al. [29] prepared a traditional NiCrAlY coating and a nanocrystalline coating on the N5 superalloy for comparative experiments, and the chemical composition of the nanocrystalline coating was consistent with that of the N5 superalloy. After oxidation at 1000 °C for 1000 h, no IDZ, SRZ and TCP phases were formed in superalloy N5 that was coated with a nanocrystalline coating, as shown in Fig. 11. In contrast, the IDZ width in the N5 superalloy coated with NiCrAlY coating is 75 μm.

In order to further develop the nanocrystalline coating, Wang et al. [64] also prepared a nanocrystalline coating with the same chemical composition as superalloy N5 on the superalloy K38G. The chemical composition of superalloy K38 and N5 nanocrystalline coating in Table 3. After oxidation at 1050 °C for 500 h, the superalloy is also free of SRZ and TCP phases, even though there are differences in the chemical composition of the coating and the superalloy.

In order to improve the thermal corrosion resistance of the nanocrystalline coating, Yang et al. [65] designed a double-layer coating: The outer layer is a NiCrAlY coating, and the inner layer is a nanocrystalline coating. After oxidation at 1050 °C for 1000 h, there was no IDZ, SRZ and TCP phases were formed in the superalloy, as shown in Fig. 12.

Oxidation Behavior

As a high-temperature protective coating, the nanocrystalline coating is expected to exhibit excellent oxidation resistance. Since its introduction in 1992, nanocrystalline coatings have been developed for various superalloys, including K17F [66], IN738 [67], K52 [68], M951 [69], K38 [60, 70] and N5 [29]. Without exception, all the nanocrystalline coatings can promote rapid growth of the protective alumina scale and avoid interdiffusion.

The latest development of nanocrystalline coating is applied to the nickel-based single crystal superalloy René N5. Wang et al. [29] deposited NiCrAlY coating and nanocrystalline coatings on superalloy René N5 for comparative experiments at 1000–1150 °C. After oxidation at 1000 and 1100 °C for 1000 h, the oxidation weight gain of the nanocrystalline coating was much lower than that of the NiCrAlY coating, less than half of it. In Fig. 13, the oxidation rate of the nanocrystalline coating applied on the single crystal superalloy René N5 and the other two traditional

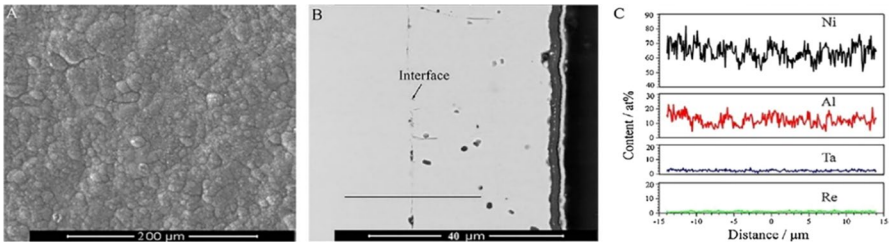

Fig. 11 Microstructure of the sputtered nanocrystalline coating after oxidation at 1100 °C for 1000 h: **a** surface morphology; **b** cross-sectional view; **c** EDS line scan at interface for elements Ni, Al, Ta, Re [29]. Reproduced from Refs. [29] with permission from the Corrosion Science ©2015, Elsevier

Table 3 Chemical composition of the superalloy K38 and N5 nanocrystalline coating (wt.%)

	Ni	C	Cr	Co	W	Mo	Al	Ti	Fe	Nb	Ta	Zr	Re
K38	Bal	0.1–0.2	15.7–16.3	8–9	2.4–2.8	1.5–2	3.2–3.7	3.0–3.5	≤0.5	0.6–1.1	1.5–2.0	0.05–0.15	–
N5	Bal		7.0	7.5	5.0	1.5	6.2				6.5		3.0

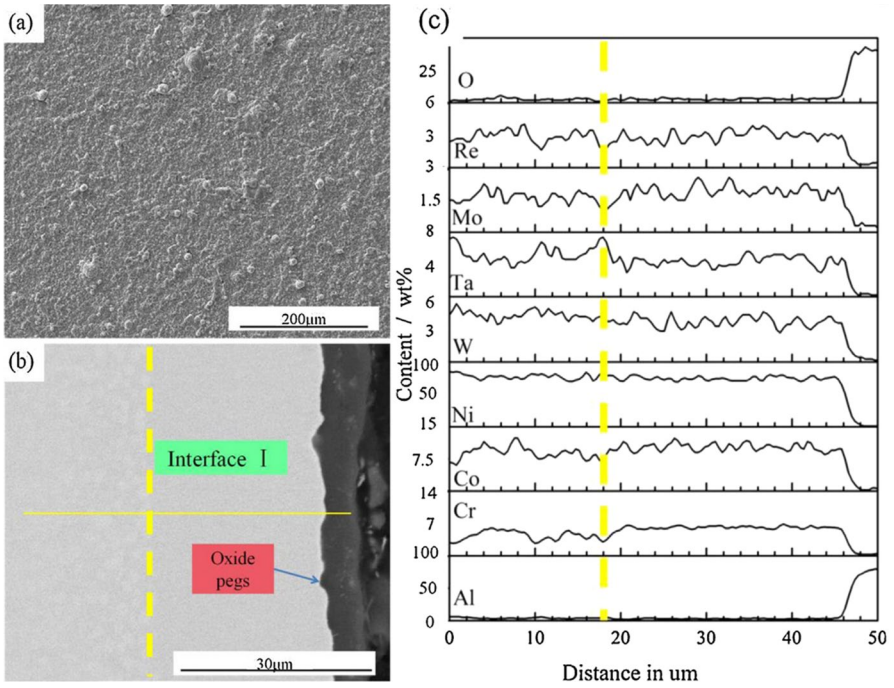

Fig. 12 Microstructures of the nanocrystalline/NiCrAlY coating after oxidation at 1050 °C for 1000 h: **a** surface; **b** cross-section; **c** EDS scanning along the yellow line in **b** [65]. Reproduced from Refs. [65] with permission from the Corrosion Science ©2016, Elsevier

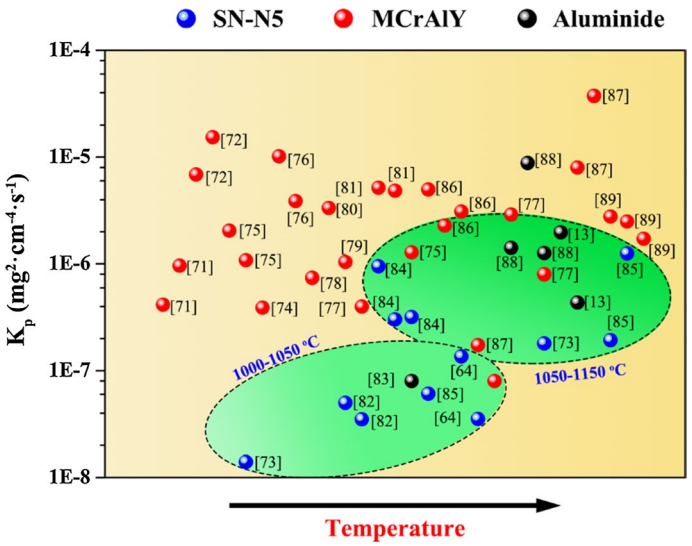

Fig. 13 Oxidation rates of the nanocrystalline coating, MCrAlY coating and aluminide coatings applied on the nickel-based superalloy René N5 at 1000–1150 °C [13, 64, 71–89]

high-temperature protective coatings (MCrAlY coating and aluminide coating) are compared. The oxidation rate of the nanocrystalline coating was much lower than that of the other two coatings. This is because the grain boundary density in the nanocrystalline coating is high, favoring high-temperature diffusion and resulting in the rapid formation of a complete Al_2O_3 scale on its surface.

More importantly, the oxide scale formed on the surface of the nanocrystalline coating exhibits excellent adhesion. The α-Al_2O_3 scale generally exhibits better oxidation resistance and lower oxidation rates compared to the Cr_2O_3 scale. However, the formation of α-Al_2O_3 easily induces the formation of voids. There are two ways to form α-Al_2O_3, directly forming α-Al_2O_3 at high temperature and transforming θ-Al_2O_3 into α-Al_2O_3. The crystal form of α-Al_2O_3 is hexagonal close-packed. When θ-Al_2O_3 is transformed into α-Al_2O_3, the volume decreases by 8–38% [90, 91]. This results in the formation of voids in α-Al_2O_3. In addition, α-Al_2O_3 scales are often prone to cracking and spalling. Indeed, the differential thermal expansion between the oxide scale and the alloy is a major factor contributing to cracking and spalling. The superalloy typically has a higher CTE compared to the oxide scale [92–94]. During cooling, the oxide scale experiences compressive stress due to the difference in thermal expansion. If the compressive stress exceeds the fracture strength of the oxide scale, it can lead to cracking and subsequent spalling of the scale. And this thermal stress can be released by creep deformation. According to the Eq. (8), the rate of creep deformation can be obtained as [95]:

$$\varepsilon = B\sigma\Omega D_b/d^3KT \tag{8}$$

σ is the tensile stress, Ω is the atomic volume, d is the average grain size, D_b is the grain boundary diffusion coefficient, δ is the grain boundary thickness, K is the Boltzmann constant, and T is the absolute temperature. The relationship described by Eq. (8) reveals that the creep rate of the oxide scale decreases as the cube of the grain diameter of the oxide scale increases. In the case of the nanocrystalline coating, the presence of grain boundaries and defects serves as abundant nucleation sites for the formation of the oxide scale on the surface. Consequently, the resulting oxide scale exhibits a small grain size [96, 97].

Therefore, nanocrystalline coatings exhibit excellent performance, whether it is inhibiting the interdiffusion between coatings and high-temperature alloys or resisting high-temperature oxidation. As a highly promising nanocrystalline coating, its current application is not yet widespread, and further development is needed to unlock its full potential.

Conclusions

Several different mean of inhibiting interdiffusion between superalloys and high-temperature protective coatings has been discussed. Diffusion barrier layer is currently the most widely used method to inhibit interdiffusion. Diffusion barriers can be classified into ceramic diffusion barriers and metal diffusion barriers. Ceramic diffusion barriers have excellent diffusion resistance but poor adhesion to both

the coating and high-temperature alloys. On the other hand, metal diffusion barriers have good adhesion to both the coating and high-temperature alloys but exhibit lower diffusion resistance. The application of EQ coatings is not yet widely popular, and their antioxidation performance is relatively poor. Nanocrystalline coatings provide a perfect solution to the problem of interdiffusion, and they exhibit better antioxidation performance compared to traditional coatings. The significant application potential of nanocrystalline coatings is yet to be fully explored and developed.

Acknowledgements This project is financially supported by the National Natural Science Foundation of China under Grant (51671053 and 51801021), the Fundamental Research Funds for the Central Universities (No. N2302007), and the Ministry of Industry and Information Technology Project (No. MJ-2017-J-99).

Author Contributions BM was contributed to methodology, conceptualization, formal analysis, visualization, writing—original draft. JW and ZB were contributed to methodology, writing—original draft. MC was contributed to funding acquisition, supervision, project administration, writing—review and editing. SZ was contributed to supervision, writing—review and editing. FW was contributed to supervision.

Data Availability All data created during this research are provided in full in the results.

Declarations

Conflict of interest The authors have no conflict of interest.

References

1. N. P. Padture, M. Gell, and E. H. Jordan, *Science* 296, 280 (2002).
2. D. R. Clarke, M. Oechsner, and N. P. Padture, *MRS Bulletin* 37, 891 (2012).
3. Z. Khan, S. Fida, F. Nisar, and N. Alam, *Engineering Failure Analysis* 68, 197 (2016).
4. Y. Chen, X. Zhao, and P. Xiao, *Acta Materialia* 159, 150 (2018).
5. W. Mo, M. Shao, Y. Wu, Q. Sun, S. Xia, F. Wen, and Y. Wang, *Journal of Vacuum Science & Technology A* 41, 043103 (2023).
6. A. Kalush, D. Texier, M. Ecochard, Q. Sirvin, K. Choquet, T. Gheno, N. Vandersees, W. Jomaa, and P. Bocher, *Surface and Coatings Technology* 440, 128483 (2022).
7. B. Wang, J. Gong, A. Y. Wang, C. Sun, R. F. Huang, and L. S. Wen, *Surface and Coatings Technology* 149, 70 (2002).
8. Y. Xu, W. Li, and X. Yang, *Corrosion Science* 196, 110033 (2022).
9. L. Yang, M. Chen, J. Wang, Y. Qiao, P. Guo, S. Zhu, and F. Wang, *Journal of Materials Science & Technology* 45, 49 (2020).
10. T. Liang, H. Guo, H. Peng, and S. Gong, *Journal of Alloy and Compounds* 509, 8542 (2011).
11. K. Matuszewski, R. Rettig, H. Matysiak, Z. Peng, I. Povstugar, P. Choi, J. Müller, D. Raabe, E. Spiecker, K. J. Kurzydłowski, and R. F. Singer, *Acta Materialia* 95, 274 (2015).
12. R. A. Hobbs, L. Zhang, C. M. F. Rae, and S. Tin, *Metallurgical and Materials Transactions A* 39, 1014 (2008).
13. C. Jiang, L. Qian, M. Feng, H. Liu, Z. Bao, M. Chen, S. Zhu, and F. Wang, *Journal of Materials Science & Technology* 35, 1334 (2019).
14. Z. Bai, D. Li, H. Peng, J. Wang, H. Guo, and S. Gong, *Progress in Natural Science: Materials International* 22, 146 (2012).
15. B. Seiser, R. Drautz, and D. G. Pettifor, *Acta Materialia* 59, 749 (2011).
16. H. Long, Y. Liu, S. Mao, H. Wei, J. Zhang, S. Ma, Q. Deng, Y. Chen, Z. Zhang, and X. Han, *Scripta Materialia* 157, 100 (2018).
17. Y. Zhao, J. Zhao, H. Long, Y. Liu, Y. Chen, S. Mao, Z. Zhang, and X. Han, *Materials Research Letters* 11, 623 (2023).

18. K. Cao, W. Yang, C. Liu, P. Qu, J. Qin, J. Zhang, and L. Liu, *Journal of Alloys and Compounds* 942, 168951 (2023).
19. W. Xia, X. Zhao, Q. Yue, W. Xuan, Q. Pan, J. Wang, Q. Ding, H. Bei, and Z. Zhang, *Materials Characterization* 187, 111855 (2022).
20. Z. Zhang and Z. Yue, *Journal of Alloys and Compounds* 746, 84 (2018).
21. C. S. Richard, G. Béranger, J. Lu, and J. F. Flavenot, *Surface and Coatings Technology* 82, 99 (1996).
22. M. Simonetti and P. Caron, *Materials Science and Engineering: A* 254, 1 (1998).
23. S. Tian, M. Wang, T. Li, B. Qian, and J. Xie, *Materials Science and Engineering: A* 527, 5444 (2010).
24. Z. Zhang, B. Gleeson, K. Jung, L. Li, and J. C. Yang, *Acta Materialia* 60, 5273 (2012).
25. N. Wanderka and U. Glatzel, *Materials Science and Engineering: A* 203, 69 (1995).
26. A. Volek, F. Pyczak, R. F. Singer, and H. Mughrabi, *Scripta Materialia* 52, 141 (2005).
27. A. Sato, Y. Aoki, M. Arai, and H. Harada, *Journal of the Japan Institute of Metals and Materials* 71, 320 (2007).
28. C. Wang, W. Chen, M. Chen, D. Chen, K. Yang, and F. Wang, *Journal of Materials Science & Technology* 45, 125 (2020).
29. J. Wang, M. Chen, L. Yang, S. Zhu, and F. Wang, *Corrosion Science* 98, 530 (2015).
30. S. H. Hosseini, S. Mirdamadi, and S. Rastegari, *Surface Engineering* 31, 146 (2015).
31. X. M. Peng, C. Q. Xia, X. Y. Dai, A. R. Wu, L. J. Dong, D. F. Li, and Y. R. Tao, *Surface and Coating Technology* 232, 254 (2013).
32. Z. Lou, Y. Li, Q. Zou, W. Luo, H. Gu, Z. Li, and Y. Luo, *Ceramics International* 49, 20849 (2023).
33. T. Luo, Z. Cao, X. Su, P. Li, and Y. Song, *Ceramics International* 49, 19149 (2023).
34. Z. Lou, Y. Li, Q. Zou, W. Luo, H. Gu, Z. Li, and Y. Luo, *Materials Characterization* 199, 112817 (2023).
35. L. Zhu, S. Zhu, and F. Wang, *Corrosion Science* 60, 265 (2012).
36. L. Zhu, C. Feng, S. Zhu, F. Wang, J. Yuan, and P. Wang, *Crystals* 11, 1333 (2021).
37. W. Z. Li, Q. M. Wang, J. Gong, C. Sun, and X. Jiang, *Applied Surface Science* 255, 8190 (2009).
38. W. Z. Li, D. Q. Yi, Y. Q. Li, H. Q. Liu, and C. Sun, *Journal of Alloys and Compounds* 518, 86 (2012).
39. H. Peng, H. Guo, J. He, and S. Gong, *Journal of Alloys and Compounds* 502, 411 (2010).
40. R. Cremer, M. Witthaut, K. Reichert, M. Schierling, and D. Neuschütz, *Surface and Coatings Technology* 108–109, 48 (1998).
41. O. Knotek, F. Löffer, and W. Beele, *Surface and Coatings Technology* 61, 6 (1993).
42. J. Müller and D. Neuschütz, *Vacuum* 71, 247 (2003).
43. O. Knotek, E. Lugscheider, F. Löffer, and W. Beele, *Surface and Coatings Technology* 68–69, 22 (1994).
44. P. Ren, S. Zhu, and F. Wang, *Corrosion Science* 99, 219 (2015).
45. Y. Cai, C. Tao, F. Lu, and J. Li, *Advanced Materials Research* 97–101, 1479 (2010).
46. S. Gao, B. He, L. Zhou, and J. Hou, *Corrosion Science* 170, 108682 (2020).
47. B. Meng, J. Wang, L. Yang, L. Zhu, M. Chen, S. Zhu, and F. Wang, *NPJ Materials Degradation* 21, 6 (2022).
48. H. Tung and J. Stubbins, *Journal of Nuclear Materials* 424, 23 (2012).
49. B. Bai, H. Guo, H. Peng, L. Peng, and S. Gong, *Corrosion Science* 53, 2721 (2011).
50. Y. Katsumata, T. Yoshioka, K. Z. Thosin, T. Nishimoto, T. Izumi, S. Hayashi, and T. Narita, *Oxidation of Metals* 68, 331 (2007).
51. C. Burman, T. Ericsson, I. Kvernes, and Y. Lindblom, *Surface and Coatings Technology* 32, 127 (1987).
52. C. Burman, T. Ericsson, I. Kvernes, and Y. Lindblom, *Surface and Coatings Technology* 36, 1 (1988).
53. F. Wu, H. Murakami, and A. Suzuki, *Surface and Coatings Technology* 168, 62 (2003).
54. E. Cavaletti, S. Naveos, S. Mercier, P. Josso, M. P. Bacos, and D. Monceau, *Surface and Coatings Technology* 204, 761 (2009).
55. F. Lang and T. Narita, *Intermetallics* 15, 599 (2007).
56. T. Narita, F. Lang, K. Z. Thosin, T. Yoshioka, T. Izumi, H. Yakuwa, and S. Hayashi, *Oxidation of Metals* 68, 343 (2007).
57. Z. Xu, P. Zhang, W. Wang, Q. Shi, H. Yang, D. Wang, Y. Hong, L. Wei, C. Guo, S. Lin, and M. Dai, *Surface and Coatings Technology* 414, 127101 (2021).
58. A. Sato, H. Harada, and K. Kawagishi, *Metallurgical and Materials Transactions A* 37, 789 (2006).
59. K. Kawagishi, A. Sato, K. Matsumoto, T. Kobayashi, H. Harada, Y. Aoki, and M. Arai, *Journal of the Japan Institute of Metals and Materials* 71, 226 (2007).
60. H. Lou, F. Wang, B. Xia, and L. Zhang, *Oxidation of Metals* 38, 299 (1992).

61. C. Wagner, *Journal of The Electrochemical Society* 99, 369 (1952).
62. X. Peng, J. Yang, Y. Zhou, and F. Wang, *Acta Materialia* 53, 5079 (2005).
63. B. Meng, J. Wang, L. Yang, M. Chen, S. Zhu, and F. Wang, *Journal of Materials Science & Technology* 132, 69 (2023).
64. J. Wang, B. Meng, W. Sun, L. Yang, M. Chen, and F. Wang, *Coatings* 10, 1188 (2020).
65. L. Yang, M. Chen, J. Wang, S. Zhu, and F. Wang, *Corrosion Science* 102, 72 (2016).
66. H. Lou, Y. Tang, X. Sun, and H. Guan, *Materials Science and Engineering: A* 207, 121 (1996).
67. S. Geng, F. Wang, and S. Zhang, *Surface and Coatings Technology* 167, 161 (2003).
68. F. Wang, X. Tian, Q. Li, L. Li, and X. Peng, *Thin Solid Films* 516, 5740 (2008).
69. X. Wang, L. Xin, F. Wang, S. Zhu, H. Wei, and X. Wang, *Journal of Materials Science & Technology* 30, 867 (2014).
70. W. Sun, M. Chen, Z. Bao, C. Wu, S. Zhu, and F. Wang, *Surface and Coatings Technology* 358, 958 (2019).
71. J. Lu, S. Zhu, and F. Wang, *Oxidation of Metals* 76, 67 (2011).
72. E. Ghadami, A. Sabour Rouh Aghdam, and S. Ghadami, *Ceramics International* 46, 20500 (2020).
73. J. Wang, M. Chen, S. Zhu, and F. Wang, *Applied Surface Science* 345, 194 (2015).
74. J. Wang, H. Ji, M. Chen, Z. Bao, S. Zhu, and F. Wang, *Corrosion Science* 175, 108894 (2020).
75. P. Zhao, M. Shen, Y. Gu, S. Zhu, and F. Wang, *Corrosion Science* 126, 317 (2017).
76. F. Ghadami, A. Zakeri, A. Sabour Rouh Aghdam, and R. Tahmasebi, *Surface and Coatings Technology* 373, 7 (2019).
77. H. Peng, H. Guo, J. He, and S. Gong, *Surface and Coatings Technology* 207, 110 (2012).
78. D. Mercier, C. Kaplin, G. Goodall, G. Kim, and M. Brochu, *Surface and Coatings Technology* 205, 2546 (2010).
79. Y. J. Zhang, X. F. Sun, Y. C. Zhang, T. Jin, C. G. Deng, H. R. Guan, and Z. Q. Hu, *Materials Science and Engineering: A* 360, 65 (2003).
80. F. J. Belzunce, V. Higuera, and S. Poveda, *Materials Science and Engineering: A* 297, 162 (2001).
81. C. Kaplin and M. Brochu, *Applied Surface Science* 301, 258 (2014).
82. J. Wang, M. Chen, L. Yang, L. Liu, S. Zhu, F. Wang, and G. Meng, *Applied Surface Science* 366, 245 (2016).
83. J. Angenete and K. Stiller, *Surface and Coatings Technology* 150, 107 (2002).
84. S. Yang, Y. Wang, M. Chen, L. Yang, J. Wang, S. Zhu, and F. Wang, *Corrosion Science* 170, 108700 (2020).
85. L. Yang, J. Wang, R. Yang, S. Yang, Y. Jia, M. Chen, Y. Qiao, P. Guo, S. Zhu, and F. Wang, *Corrosion Science* 180, 109182 (2021).
86. L. Ni, Z. Wu, and C. Zhou, *Progress in Natural Science: Materials International* 21, 173 (2011).
87. H. Yang, J. Zou, Q. Shi, D. Wang, M. Dai, S. Lin, X. Chen, W. Wang, and X. Xia, *Corrosion Science* 175, 108889 (2020).
88. Y. F. Yang, C. Y. Jiang, Z. B. Bao, S. L. Zhu, and F. H. Wang, *Corrosion Science* 106, 43 (2016).
89. J. Sun, H. Xiao, W. Li, S. B. Liu, L. B. Fu, and S. M. Jiang, *Surface and Coatings Technology* 399, 126164 (12020).
90. J. M. Alvarado-Orozco, R. Morales-Estrella, M. S. Boldrick, G. Trapaga-Martinez, B. Gleeson, and J. Munoz-Saldana, *Metallurgical and Materials Transactions A* 46, 726 (2015).
91. T. F. An, H. R. Guan, X. F. Sun, and Z. Q. Hu, *Oxidation of Metals* 54, 301 (2000).
92. L. Qiu, F. Yang, W. Zhang, X. Zhao, and P. Xiao, *Corrosion Science* 89, 13 (2014).
93. L. Yang, L. Zheng, and H. Guo, *Corrosion Science* 112, 542 (2016).
94. C. Li, X. Zhang, Y. Chen, J. Carr, S. Jacques, J. Behnsen, M. Michiel, P. Xiao, and R. Cernik, *Acta Materialia* 132, 1 (2017).
95. J. Karch, R. Birringer, and H. Gleiter, *Nature* 330, 556 (1987).
96. H. Lou, F. Wang, S. Zhu, B. Xia, and L. Zhang, *Surface and Coatings Technology* 63, 105 (1994).
97. J. Wang, M. Chen, L. Yang, W. Sun, S. Zhu, and F. Wang, *Corrosion Communications* 1, 58 (2021).